ELECTRONIC SUPPLEMENTARY INFORMATION (ESI)

Water-soluble ionic carbon nitride as unconventional stabilizer for highly catalytically active ultrafine gold nanoparticles

Mohamed M. Elnagar,[a]‡ Johannes Liessem, [a]‡ Changbin Im,[a]‡ Dariusz Mitoraj,[a] Ludwig A. Kibler,[a] Christof Neumann,[b] Andrey Turchanin,[b] Robert Leiter,[c] Ute Kaiser,[c] Timo Jacob,[a,d,e]* Igor Krivtsov,[a, f]* Radim Beranek[a]*

[a] Institute of Electrochemistry Ulm University, Albert-Einstein-Allee 47, 89081 Ulm, Germany

[b] Institute of Physical Chemistry, Jena Center for Soft Matter (JCSM) and Center for Energy and Environmental Chemistry Jena (CEEC), Friedrich Schiller University Jena, Lessingstr. 10, 07743 Jena, Germany

[c] Electron Microscopy of Materials Science, Central Facility for Electron Microscopy, Ulm University, Albert-Einstein-Allee 11, 89081, Ulm, Germany

[d] Helmholtz-Institute-Ulm (HIU) Electrochemical Energy Storage, Helmholtzstr. 11, 89081, Ulm, Germany

[e] Karlsruhe Institute of Technology (KIT), P.O. Box 3640, 76021, Karlsruhe, Germany

[f] Department of Chemical and Environmental Engineering, University of Oviedo, 33006 Oviedo, Spain

*Corresponding authors: Radim Beranek (radim.beranek@uni-ulm.de), Timo Jacob (timo.jacob@uni-ulm.de), Igor Krivtsov (krivtsovigor@uniovi.es)

1. Materials and Methods

1.1 Materials and chemicals

Melamine (99 %, Sigma Aldrich), dicyandiamide (99%, Sigma Aldrich), cyanuric acid (98 %, Sigma Aldrich), KOH and NaOH (Merck, 99 %), and potassium thiocyanate (KSCN) (98%, Merk) were used for the synthesis of the stabilizers. Hydrogen tetrachloroaurate ($HAuCl_4.3H_2O$) (49 wt% Au basis, Alfa Aesar) and sodium borohydride ($NaBH_4$) (≥ 96%, Sigma Aldrich) were utilized for the synthesis of Au NPs. All chemicals were used as received without further purification unless otherwise specified.

1.2. Synthesis

1.2.1. Synthesis of the proposed stabilizers

K, Na KPHI. We synthesized the K, Na PHI according to our previously reported method.[1] In brief, 10 mmol KOH (56 g mol^{-1}) and 5 mmol NaOH (40 g mol^{-1}) were ground and mixed with 12 mmol melamine (126 g mol^{-1}). The powder was then heated in a lid-covered crucible at a rate of 5.0 °C min^{-1} up to 330 °C, then it was kept for 2h at the reached temperature before being withdrawn from the furnace. The obtained solid was suspended in 100 mL of deionized water and the insoluble part was filtered out, firstly, by a paper filter and afterward by a 0.2 µm PTFE syringe filter. The obtained solution was dialyzed for several days until neutral pH values, and concentrated by evaporation at 60 °C to a concentration of 5.0 g L^{-1}, which was determined gravimetrically. To obtain solid material of the water-soluble K, Na PHI, the solution was gradually evaporated at 60 °C and then dried for 24 h at 80 °C. The FTIR spectrum shown in **Figure S1a** demonstrates the successful synthesis of K, Na PHI.

Tripotassium melonate. Tripotassium melonate (KMel) was synthesized by a modified procedure described by Schlomberg *et al.* [2] Firstly, the melon polymer was synthesized by dicyandiamide condensation in an open crucible at 550 °C for 4.0 h and the obtained solid was washed with deionized water and dried at 70 °C. Then, 1.5 g of melon polymer was mixed and ground with 3.0 g of KSCN (30.9 mmol, 97 g mol^{-1}). The mixture was heated in a lid-covered crucible at a rate of 5.0 °C min^{-1} up to 550 °C for 4h. The obtained solid was suspended in 50 mL of water, then filtered through a paper filter and through a

syringe 0.2 µm filter to remove solid impurities. The solution was slowly evaporated to a small volume yielding a white powder. The powder was recovered by filtration and washed with ethanol. The FTIR and ^{13}C NMR spectra shown in **Figure S1b,c** demonstrate the successful synthesis of the melonate anion.

Tripotassium cyamelurate. For the synthesis of tripotassium cyamelurate (KCya), 1.0 g of melon was suspended in 1.0 mol L^{-1} solution of KOH and hydrothermally treated in a Teflon-lined stainless-steel autoclave for 16 h at 100 °C. After the treatment, the autoclave was cooled down to room temperature, the solution was filtered through a paper filter to remove undissolved melon and then was slowly evaporated to yield needle-shaped crystals of tripotassium cyamelurate. The ^{13}C NMR spectrum of tripotassium cyamelurate is shown in **Figure S1d.**

Tripotassium cyanurate. Tripotassium cyanurate (KCA) was obtained by stirring KOH and cyanuric acid in a stoichiometric ratio of 3:1 till complete dissolution.

1.2.2. Synthesis of Au NPs

Borohydride-based Au nanoparticle synthesis. Au NPs stabilized by BH_4^- were synthesized using a method similar to that described by Deraedt *et al.*[3], in which Au^{3+} ions are reduced by BH_4^- in an aqueous solution of $HAuCl_4$ and $NaBH_4$. In a typical experiment, the Au NPs stabilized by the proposed stabilizers were synthesized as follows at room temperature (19-22 °C). For the synthesis of each sample, 10 mL of 2.5×10^{-4} mol L^{-1} $HAuCl_4 \cdot 3H_2O$ (393.8 g mol^{-1}) was placed in a screw cover glass vial. The solutions were diluted up to 14 mL with deionized water and stirred for 5.0 min. Afterward, 1.0 mL of various concentrations of $NaBH_4$ (5.0×10^{-3} mol L^{-1}, 2.5×10^{-2} mol L^{-1} , 5.0×10^{-2} mol L^{-1} or 1.25×10^{-1} mol L^{-1}) was added dropwise under stirring to set the $NaBH_4$:$HAuCl_4$ molar ratios to 2.0, 10, 20, or 50, respectively. Upon addition, an immediate color change was observed, indicating the formation of Au NPs.

Stabilizers-based Au nanoparticle synthesis. Au NPs stabilized by the proposed stabilizers were synthesized using the same aforementioned steps, but with adding the proposed stabilizers and stirring for 5.0 min before the reduction step by $NaBH_4$. For this, various volumes of a specific concentration of the stabilizer (2.5×10^{-2} mol L^{-1} in the case of KMel, KCya, or KCA, and 3.0 g L^{-1} in the case of K,Na PHI) were added to have

different $HAuCl_4$: stabilizer ratios. For the reduction step, 1.0 mL of 2.5×10^{-2} $NaBH_4$ ($NaBH_4$:$HAuCl_4$ molar ratio of 10) was added dropwise under stirring. **Table S1** summarizes the final concentrations of $HAuCl_4$, stabilizer, and $NaBH_4$ in the synthesized materials and their corresponding names.

Dialysis step: For reduction of the ionic strength, the Au NPs were put in a cellulose membrane with a pore size of 3.5 kDa and dialyzed against H_2O for about a week.

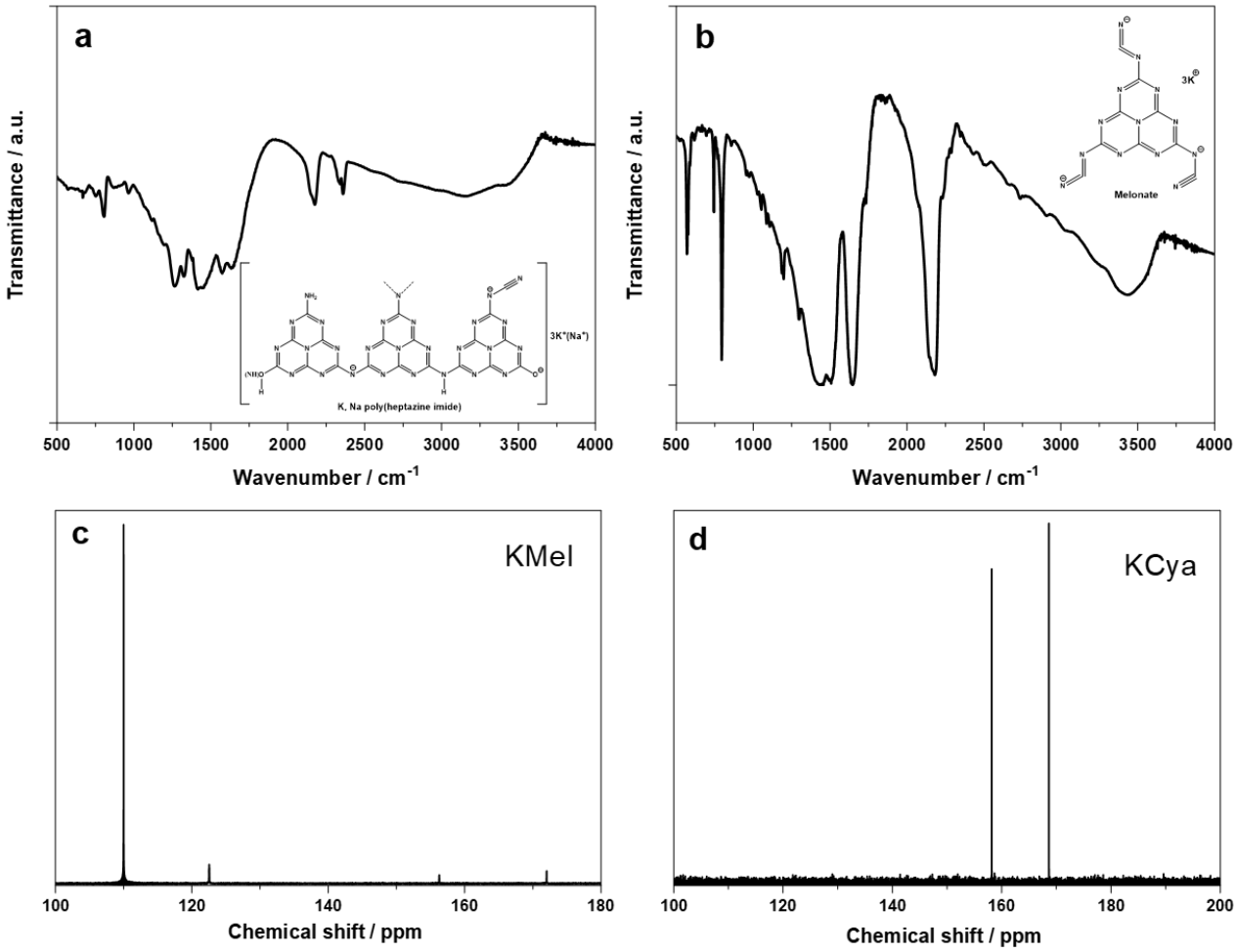

Figure S1. FTIR spectra of (a) K, Na PHI and (b) KMel, and ^{13}C NMR of (c) KMel and (d) KCya.

Table S1. The final concentrations of $HAuCl_4$, stabilizer, and $NaBH_4$ in the synthesized materials and their corresponding names.

Sample name	$HAuCl_4$ concentration / mol L^{-1}	Stabiliser	[Stabilizer : $HAuCl_4$]	$NaBH_4$: $HAuCl_4$ molar ratio
Au2	1.67×10^{-4}	-	-	2
Au10	1.67×10^{-4}	-	-	10
Au20	1.67×10^{-4}	-	-	20
Au50	1.67×10^{-4}	-	-	50
		K, Na PHI / g L^{-1}		
Au10	1.67×10^{-4}	-	-	10
K,NaPHI1	1.67×10^{-4}	1.49×10^{-2}	-	10
K,NaPHI2	1.67×10^{-4}	3.72×10^{-2}	-	10
K,NaPHI3	1.67×10^{-4}	7.43×10^{-2}	-	10
K,NaPHI4	1.67×10^{-4}	1.49×10^{-1}	-	10
K,NaPHI5	1.67×10^{-4}	2.97×10^{-1}	-	10
		KMel/KCya/KCA / mol L^{-1}		
KMel0.1	1.67×10^{-4}	1.67×10^{-5}	1 : 10	10
KMel0.3	1.67×10^{-4}	5.58×10^{-5}	1 : 3	10
KMel1	1.67×10^{-4}	1.67×10^{-4}	1 : 1	10
KMel10	1.67×10^{-4}	1.67×10^{-3}	10 : 1	10
KCya0.1	1.67×10^{-4}	1.67×10^{-5}	1 : 10	10
KCya0.3	1.67×10^{-4}	5.58×10^{-5}	1 : 3	10
KCya1	1.67×10^{-4}	1.67×10^{-4}	1 : 1	10
KCya10	1.67×10^{-4}	1.67×10^{-3}	10 : 1	10
KCA0.1	1.67×10^{-4}	1.67×10^{-5}	1 : 10	10
KCA0.3	1.67×10^{-4}	5.58×10^{-5}	1 : 3	10
KCA1	1.67×10^{-4}	1.67×10^{-4}	1 : 1	10
KCA10	1.67×10^{-4}	1.67×10^{-3}	10 : 1	10

1.3 Nitrophenol reduction catalysis

For the reduction of 4-NP, $NaBH_4$ was added in excess (circa 600 times) compared to 4-NP to ensure pseudo-first-order kinetics. In brief, 0.1 mL $NaBH_4$ (2.16 mol L^{-1}), 0.3 mL 4-NP (1.2×10^{-3} mol L^{-1}), and 2.5 mL deionized water were mixed in a 3 mL quartz cell. Then, the first spectrum was recorded, followed by the addition of 0.025 mL Au NP catalyst (1.14 mg L^{-1}) and shaking the cuvette quickly before recording the subsequent spectra.[4,5] The spectra were taken over a range of 10-15 minutes, where the progress of the reaction was tracked by monitoring the change in intensity of the 4-NP peak at 400 nm as a function of time. The TOF values were calculated considering the reaction data points after the initiation period and from the range that could be fitted with a linear function. The unit of TOF value is $h^{-1}\,atom_{Au}^{-1}$, as illustrated by the following equation:

$$\frac{mol(4NP)}{mol(Au) \cdot h}$$

1.4 Characterization

UV-vis spectra of the synthesized Au NPs were recorded using a Cary 60 (Agilent Technologies) spectrophotometer. The cuvettes were cleaned using aqua regia between the measurements of different samples. The DLS measurements were performed using Zetasizer Nano ZS (Malvern Instruments Ltd., UK), equipped with a 633 nm solid-state He−Ne laser and operating at a detection angle of 173.5°. The Zeta potential measurements were conducted using a Zetasizer Pro from Malvern Panalytical by Mixed-Mode Measurement phase analysis light scattering (M3-PALS) using a disposable folded capillary cell (DTS1070) in a diameter range of 3.8 nm – 100 µm. Each zeta potential measurement was carried out in triplicate, and the error was quantified as the standard deviation. Analyses were carried out in water (viscosity: 0.8872 Cp; refractive index: 1.33). The TEM images were obtained using the SALVE instrument at 80 kV acceleration voltage and the Philips CM20 at 200kV. For XPS analysis, the measurements were performed using a UHV Multiprobe system (Scienta Omicron, Germany) with a monochromatic X-ray source (Al K_α) and an electron analyzer (Argus CU) with 0.6 eV

energy resolution. Charge compensation during data acquisition was realized by an electron flood gun (NEK 150SC, Staib, Germany) at 6 eV and 50 μA. All samples were prepared by drop-casting on cleaned Si wafers with native oxide. The spectra were afterward calibrated using the Si 2p peak at 99.4 eV. The Au 4f spectra were fitted using the symmetric Voigt function (Gauß-Lorentz, GL) and an asymmetric fit, also based on Voigt functions. The asymmetric fit matches well with the data. The oxygen signal in the elemental composition is not reliable, as also a thin oxidized layer is on top of the Si-substrate. FTIR spectra of the stabilizers were recorded by a Shimadzu IRTracer-100 spectrometer at a resolution of 4 cm^{-1} from the samples powdered and pressed into KBr pellets. ^{13}C NMR spectra of KCya and KMel were acquired with a Bruker Avance III 400 spectrometer after dissolving in D_2O.

1.5. Computational details

All calculations of the carbon nitride model structures were performed using the ORCA package version 5.0.4.[6,7] The PBE0 functional, def2-TZVP basis set, def2/J auxiliary basis set, and DFT-D3 dispersion correction were used.[8–10] Then, the time-dependent DFT calculations of the ground-state geometry were performed using the PBE0 functional to obtain more precise unoccupied orbitals with 50 roots. Fukui functions were calculated to describe the frontier orbitals and the condensed Fukui function was obtained to find local reactivity using the following equations:[11–13]

$$f^+ = \rho_{N+1}(\mathbf{r}) - \rho_N(\mathbf{r}) \text{ for nucleophilic reactions}$$

$$f^- = \rho_N(\mathbf{r}) - \rho_{N-1}(\mathbf{r}) \text{ for electrophilic reactions}$$

The dual descriptor is combined with two Fukui functions to identify the nucleophilic (negative) and the electrophilic (positive) site.

$$f(r) = f^+ - f^-$$

The condensed Fukui functions can also be applied to atomic charges from a Hirshfeld analysis in order to describe the local chemical reactivity.

$$f_k^+ = q_k(N+1) - q_k(N)$$

$$f_k^- = q_k(N) - q_k(N-1)$$

where, $\rho(\mathbf{r})$ is the electron density from DFT calculations and N is the total number of electrons for the system. The condensed Fukui functions are normalized to obtain the dual descriptor.

2. Results and discussion

2.1 Synthesis and characterization of the $NaBH_4$-stabilized Au NPs

The concentration of $NaBH_4$ is a crucial parameter enabling the formation of stable Au NPs and avoiding their immediate precipitation after the synthesis.[3] To optimize the $NaBH_4$:HAuCl ratio, the concentration of $HAuCl_4$ was set as 1.67×10^{-4} mol $L^{-1,}$ and various concentrations of $NaBH_4$ were added (2.0, 10, 20, or 50 $NaBH_4$:$HAuCl_4$ molar ratio to produce **Au2**, **Au10**, **Au20**, or **Au50,** respectively). The optical images of the Au NPs after 24 hours of their synthesis using various $NaBH_4$ concentrations are shown in **Figure S2**. The four suspensions are of different colors, which implies the formation of Au NPs with different particle sizes. Accordingly, one could expect that the particle size is increasing in the sequence of **Au50** > **Au2** > **Au10** or **Au20**.[3] The **Au50** sample turns dark grey after approximately 2.0 h from the synthesis, indicating the rapid agglomeration of the particles.

Figure S3a presents the UV-vis spectra recorded for the synthesized materials on the day of the synthesis and after 21 days of storage at ambient conditions. The **Au10** and **Au20** samples exhibit very similar UV-vis spectra characterized by a narrow surface plasmon resonance (SPR) peak centered at 513 nm. There are no detectable changes in the SPR peak of these samples for at least 21 days (Figure S3a), indicating high colloidal stability. Contrary, the SPR peak for **Au2** is broader and red-shifted to 531 nm, and it becomes even broader and less intense after 21 days, while **Au50** does not show any SPR peak after about 2.0 h from its synthesis (Figure S3a). A complete agglomeration and precipitation of **Au50** is observed after 21 days, so its spectrum could not be recorded. These observations indicate the agglomeration of the Au NPs synthesized using $NaBH_4$:$HAuCl_4$ molar ratios of 2.0 and 50, which is confirmed by the high absorbance intensity in the 600-800 nm range. The stabilization ability of $NaBH_4$ at optimum concentrations is due to the electrostatic stabilization that arises from the presence of a sufficient number of deprotonated anionic species on the surface of NPs.[3] The partial

agglomeration at low $NaBH_4$ concentrations (<10 molar ratio $NaBH_4$:$HAuCl_4$) might be due to the insufficient number of anions (BH_4^-) required for the effective electrostatic stabilization of Au NPs. However, the rapid agglomeration of Au NPs at higher $NaBH_4$ concentration (>20 molar ratio $NaBH_4$:$HAuCl_4$) is induced by the decrease of surface potential that results from the electron injection into the Au NPs upon adding excess $NaBH_4$.[3,14,15] Thus, we have selected $NaBH_4$:$HAuCl_4$ molar ratio 10 as the optimum $NaBH_4$ concentration to produce ligand-free and stable Au NPs.

The effect of K,Na-PHI on the properties of Au NPs was investigated at different PHI concentrations of 1.49×10^{-2}, 3.72×10^{-2}, 7.43×10^{-2}, 1.49×10^{-1}, and 2.97×10^{-1} g L^{-1}, yielding the samples denoted as **K,NaPHI1**, **K,NaPHI2**, **K,NaPHI3**, **K,NaPHI4**, and **K,NaPHI5**, respectively. As shown in Figure S2, the five K,Na-PHI-stabilized Au NPs have a red-brownish colour that is different from that of the **Au10** $NaBH_4$-capped samples, indicating that the addition of K,Na-PHI possibly affects the particle size. Furthermore, the presence of K,Na-PHI, independent of its concentration, leads to a broad peak between 490 nm and 530 nm in the UV-vis electronic absorption spectra, which is in stark contrast to the sharp and intense SPR peak of **Au10** at 513 nm (Figure S3b). This indicates that the average particle size of all K,Na-PHI-stabilized Au NPs might be below 3 nm since larger particles would exhibit a sharper and more intense SPR peak.[16,17]

The effect of KMel, KCya, and KCA on the produced Au NPs has been investigated at different molar ratios (Stabilizer : $HAuCl_4$ = 10, 3, 1, or 0.1) with the corresponding sample designations (Table S1).

As shown in **Figure S2**, the color of the melonate and cyamelurate stabilized Au NPs is comparable to the color of K,NaPHI series except for **KMel10** and **KCya10** which have a reddish and dark grey colors, respectively. On the other hand, the cyanurate stabilized Au NPs exhibit almost the same color as **Au10**, but **KCA10** possesses a reddish color. These macroscopic differences imply that adding 10 molar excess of KMel, KCya, or KCA results in bigger AuNPs, which are expected to be agglomerated, compared to **Au10**. The UV-vis spectra reveal that the particle size of Au NPs varies as a function of the concentration of melonate added (**Figure S3c**). Notably, the particle size of **KMel0.1** and **KMel10** appears to be larger than that of **KMel0.3** and **KMel1**, the SPR peak is sharper and more intense. Furthermore, the SPR peak of **KMel10** is sharper and red-shifted by

about 10 nm than that of **Au10**, which is a clear indication of the beginning of an aggregation phenomenon. In the case of the cyamelurate–stabilized Au NPs, similar behavior is detected for the Au NPs stabilized by 0.1 and 0.3 molar ratio of KCya demonstrated by a less pronounced SPR peak compared to **Au10** (**Figure S3d**). Despite the absorbance of **KCya1** being significantly reduced over the whole spectrum, it displays a sharp SPR peak similar to **Au10,** suggesting a comparable particle size**.** Differently, increasing the concentration of KCya to reach stabilizer:$HAuCl_4$ molar ratio of 10 (**KCya10**) induces the agglomeration of the Au NPs, as revealed by the broadening of the spectrum and the high absorbance intensity at 800 nm. Interestingly, the SPR peak of **KCA0.1** and **KCA0.3** is nearly identical to **Au10** while, the SPR peak of **KCA1** and **KCA10** is red-shifted by approximately 5.0 nm and 18 nm, respectively (**Figure S3e**). These shifts imply that higher concentrations of cyanurate cause the formation of Au NPs with larger particle size.[16]

Figure S2. Optical images of Au NPs stabilized by $NaBH_4$, K,Na PHI, KMel, KCya, and KCA as a function of the concentration of the stabilizer. The code of each sample is shown above its optical image. The concentration of $HAuCl_4$, stabilizer, and $NaBH_4$ in the synthesized materials is listed in Table S1.

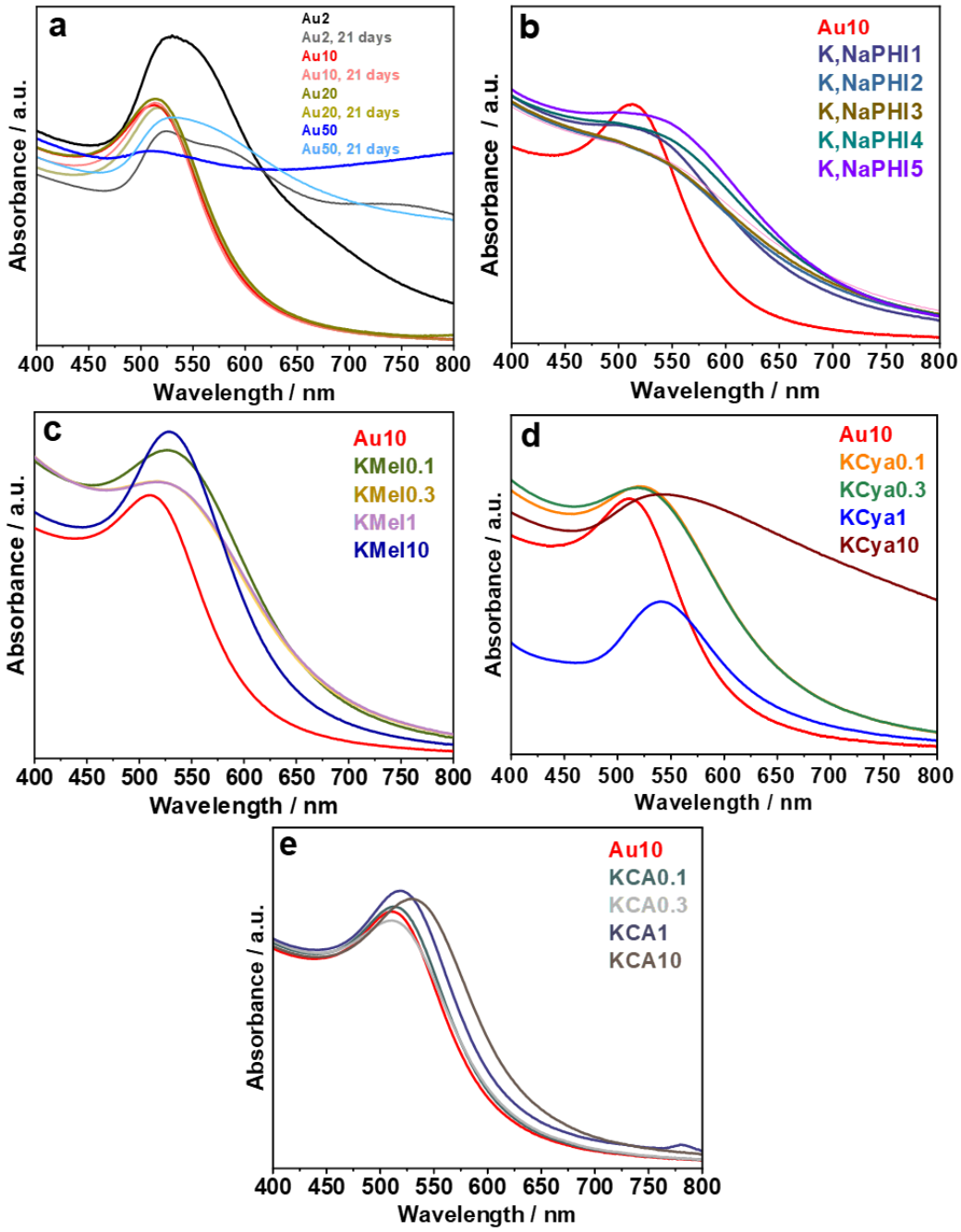

Figure S3. UV−vis absorption spectra of Au NPs stabilized by (a) $NaBH_4$ after synthsis and after 21 days of storage, (b) K,Na-PHI, (c) KMel, (d) KCya, and (e) KCA as a function of the concentration of the stabilizer.

2.2. Materials characterization

Particle size distribution

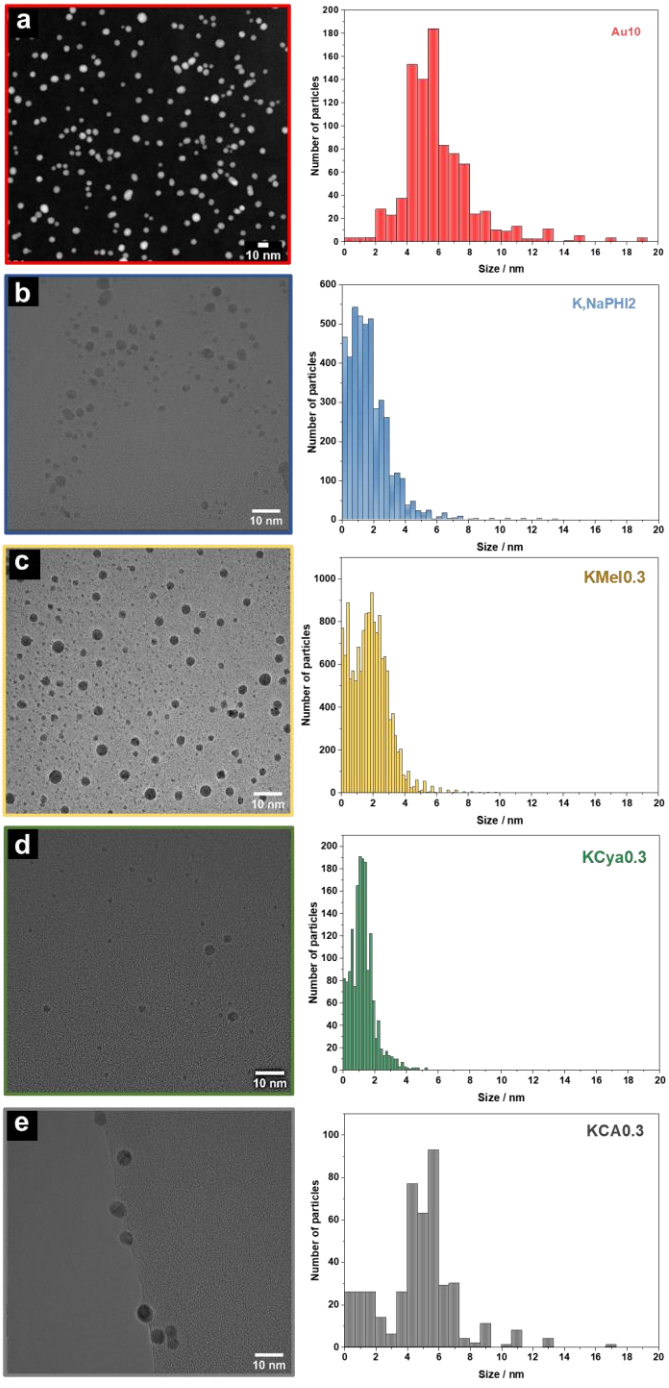

Figure S4. (S)TEM images and particle size distribution derived from the (S)TEM measurements for (a) **Au10**, (b) **K,NaPHI2**, **(**c) **KMeI0.3**, (d) **KCA0.3**, and (e) **KCya0.3**.

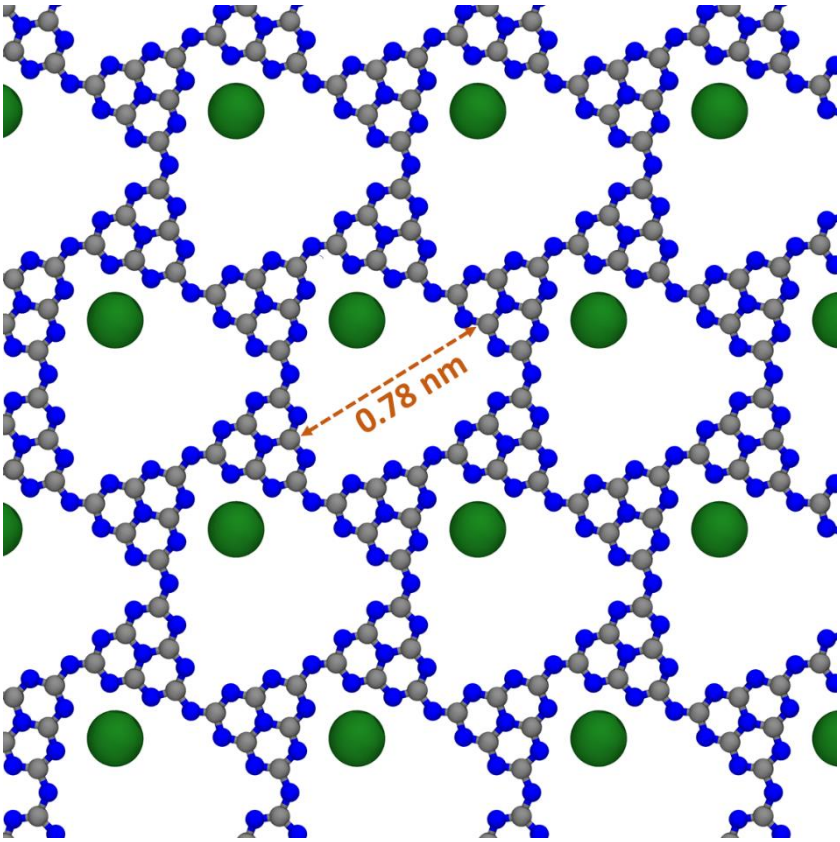

Figure S5. Schematic representation of K, Na-PHI structure highlighting the heptazine cages.

Note on XPS analysis

Figure S6a-e compares XP overview spectra (survey) of all synthesized samples. From the survey spectrum of **Au10**, the peaks corresponding to Au, B, and Na are detected. In addition to these peaks, the peaks of K and N corresponding to the proposed stabilizers are observed. The detection of the carbon peak even in **Au10** might be due hydrocarbon adsorption on the sample or carbonate formation in the basic Au NP suspensions.

The high-resolution spectra of N 1s of the synthesized samples are shown in Figure S7. As expected, **Au10** does not contain any nitrogen peak (Figure S7a). In contrast to this, the N 1s spectrum of **K,NaPHI2** exhibits three bands at 399.1, 400.6, and 405.1 eV which can be assigned to C-N=C and the sum of N-(C3), C-NH-C, as well as the π excitation, respectively (Figure S7b).[1,18,19] The N 1s spectrum of **KMel0.3** is comparable, where the intense peak at 399.3 eV is due to the overlapping of the peaks corresponding to the C-

N=C groups and cyanamide moieties (N≡C), as shown in Figure S7c. Additionally, the peak at 401.2 eV is correlated to the central N atoms in heptazines (N-(C3)). In the N 1s spectrum of **KCya0.3**, one can distinguish two peaks attributed to the C-N=C groups in the heptazines (398.9 eV) and the sum of the N-(C3) and N-C-O$^-$ species (400.6 eV) (Figure S7d). Furthermore, **KCA0.3** exhibits a low-intensity peak centered at 400.6 eV corresponds to the N atoms in deprotonated cyanuric acid (Figure S7e).

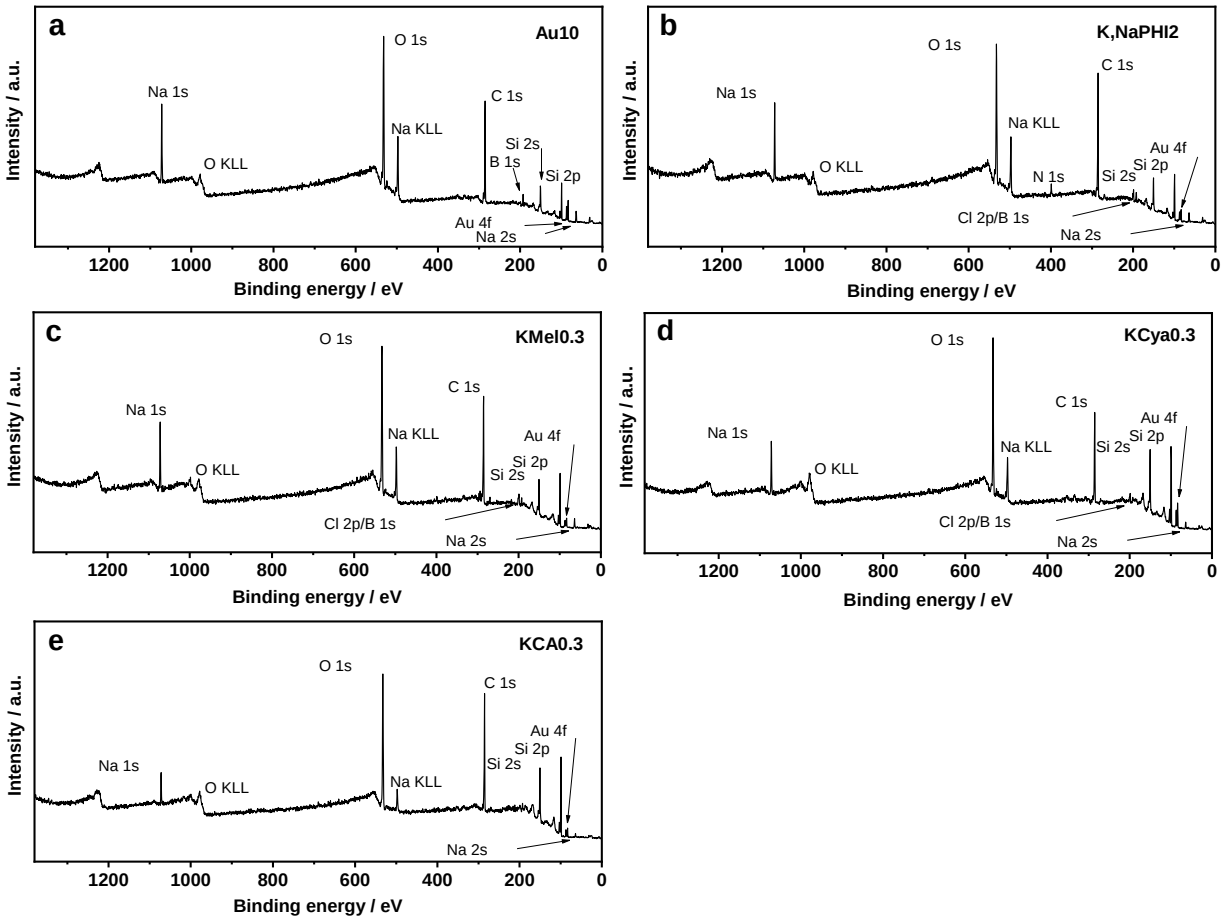

Figure S6. X-ray photoelectron survey spectra of (a) **Au10**, (b) **K,NaPHI2**, (c) **KMel0.3**, (d) **KCA0.3**, and (e) **KCya0.3**.

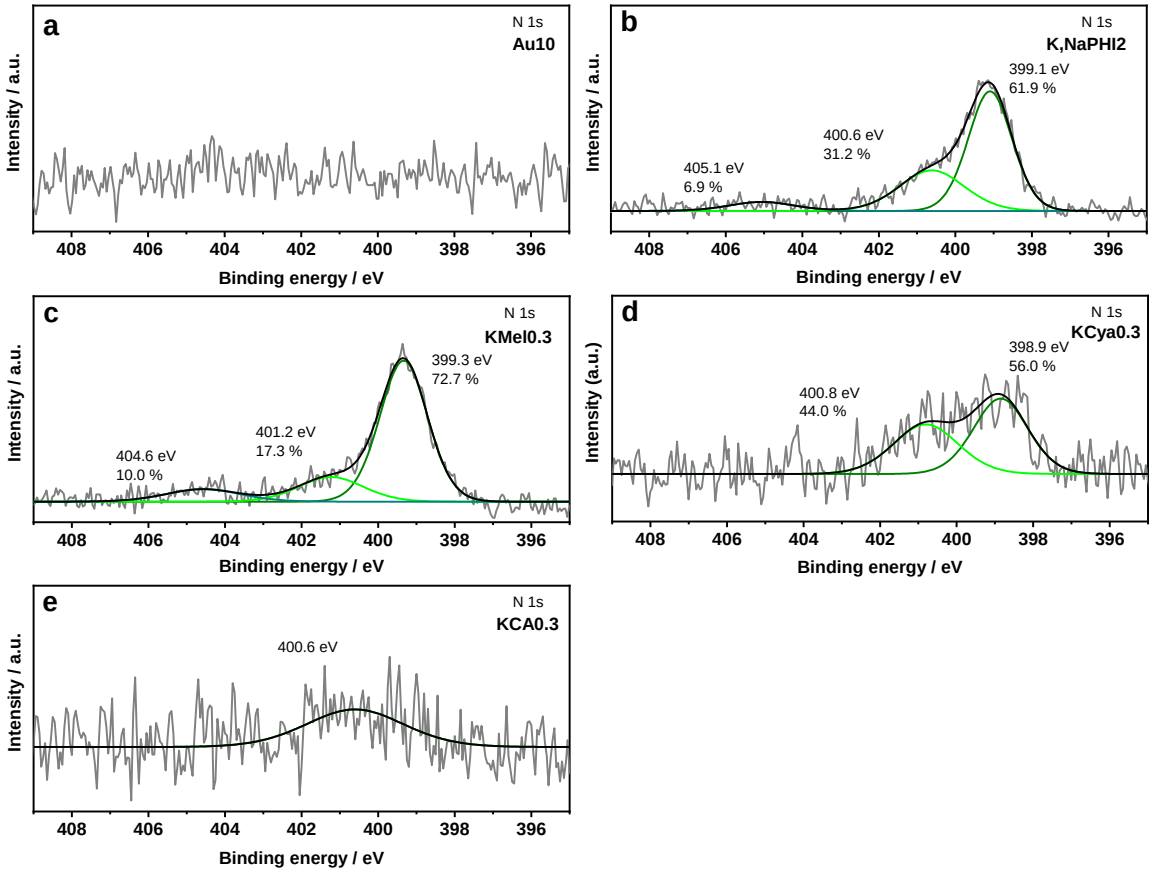

Figure S7. High-resolution N 1s XP spectra of (a) **Au10**, (b) **K,NaPHI2**, **(**c) **KMel0.3**, (d) **KCA0.3**, and (e) **KCya0.3**.

Table S2. Binding energy and full width at half maximum of the Au 4f peaks for the synthesized samples.

Sample		Binding energy / eV	Full width at half maximum / eV
Au10	Au $4f_{7/2}$	83.6	0.7
	Au $4f_{5/2}$	87.3	
K,NaPHI2	Au $4f_{7/2}$	83.6	0.8
	Au $4f_{5/2}$	87.3	
KCya0.3	Au $4f_{7/2}$	83.7	0.8
	Au $4f_{5/2}$	87.4	
KCA0.3	Au $4f_{7/2}$	83.7	0.8
	Au $4f_{5/2}$	87.4	
KMel0.3	Au $4f_{7/2}$	83.7	0.7
	Au $4f_{5/2}$	87.4	

Long-term stability of Au NPs

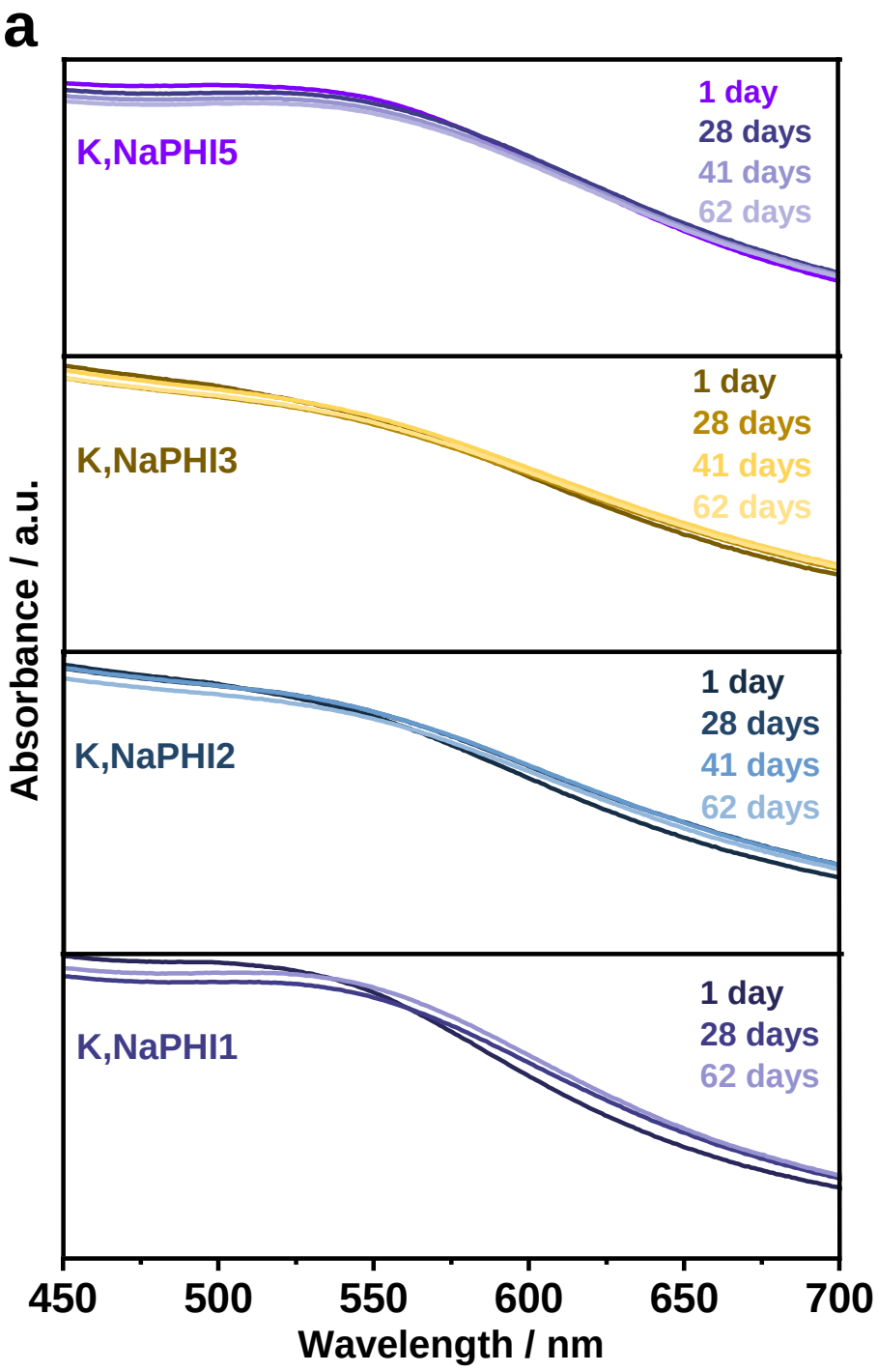

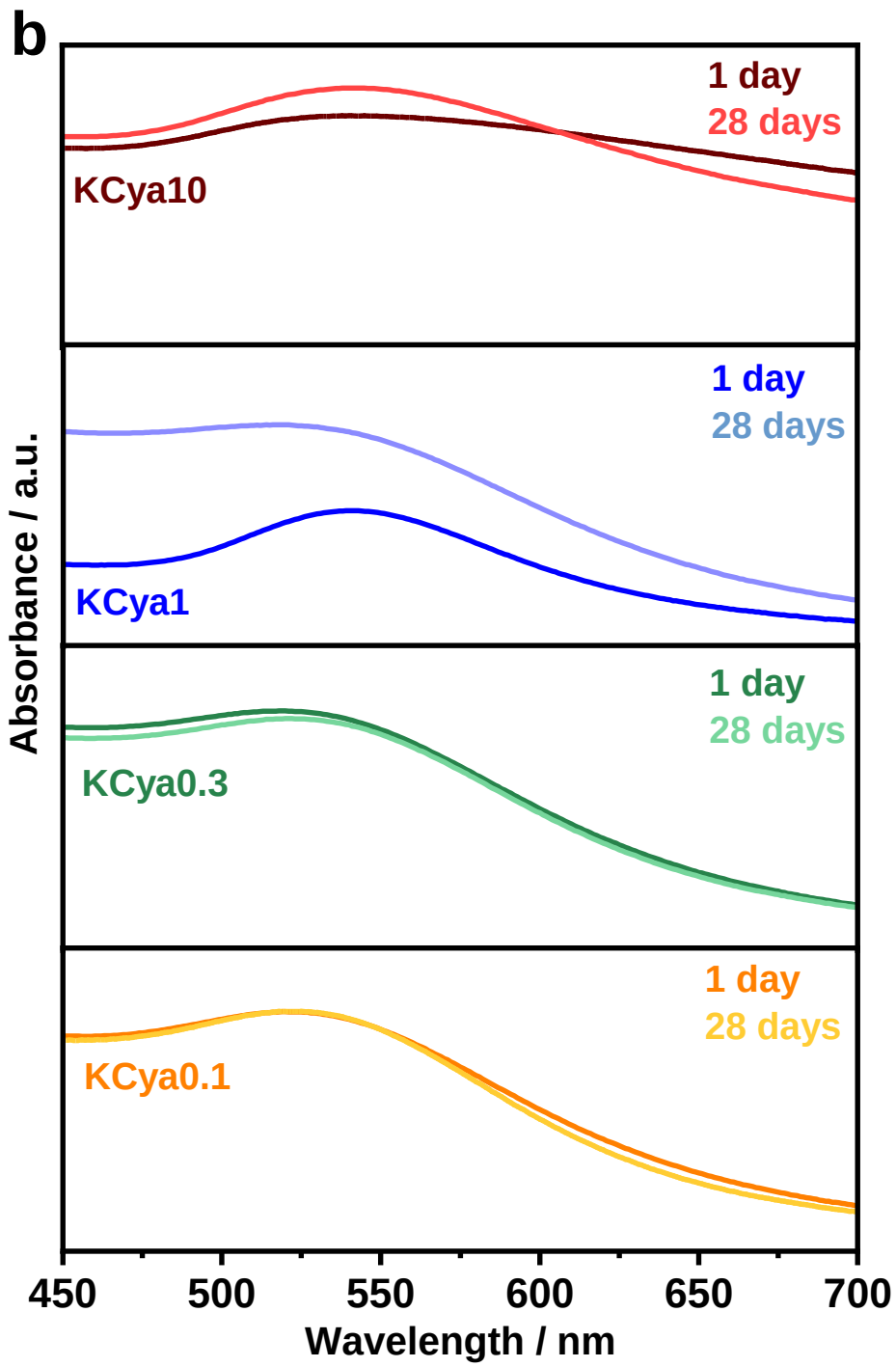
b
1 day
28 days
KCya10
1 day
28 days
KCya1
1 day
28 days
KCya0.3
1 day
28 days
KCya0.1
Absorbance / a.u.
450
500
550
600
650
700
Wavelength / nm

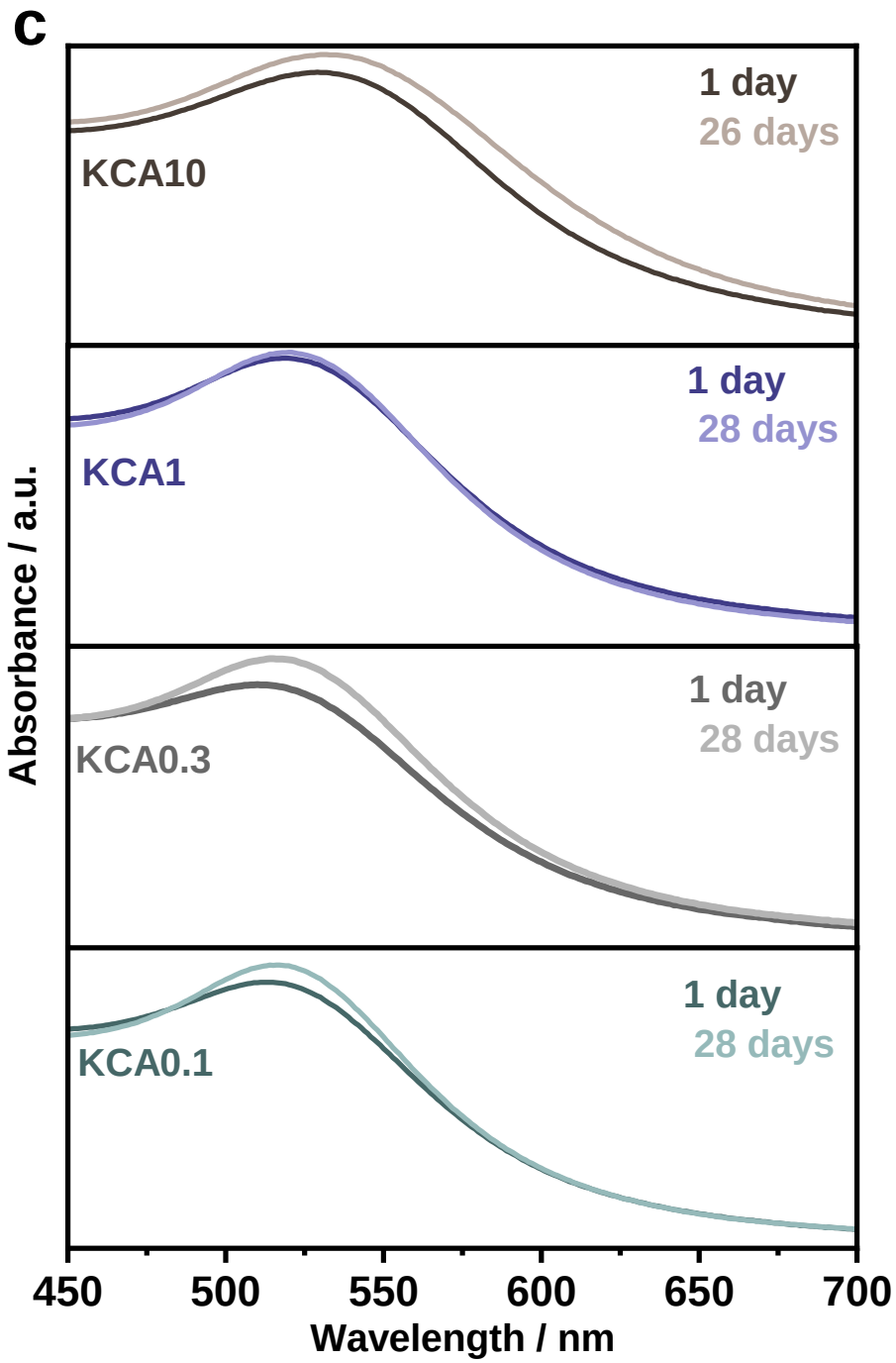

Figure S8. UV−vis absorption spectra of Au NPs produced in the presence of different concentrations of (a) K, Na PHI, (b) KCya, and (c) KCA as a function of the storage time.

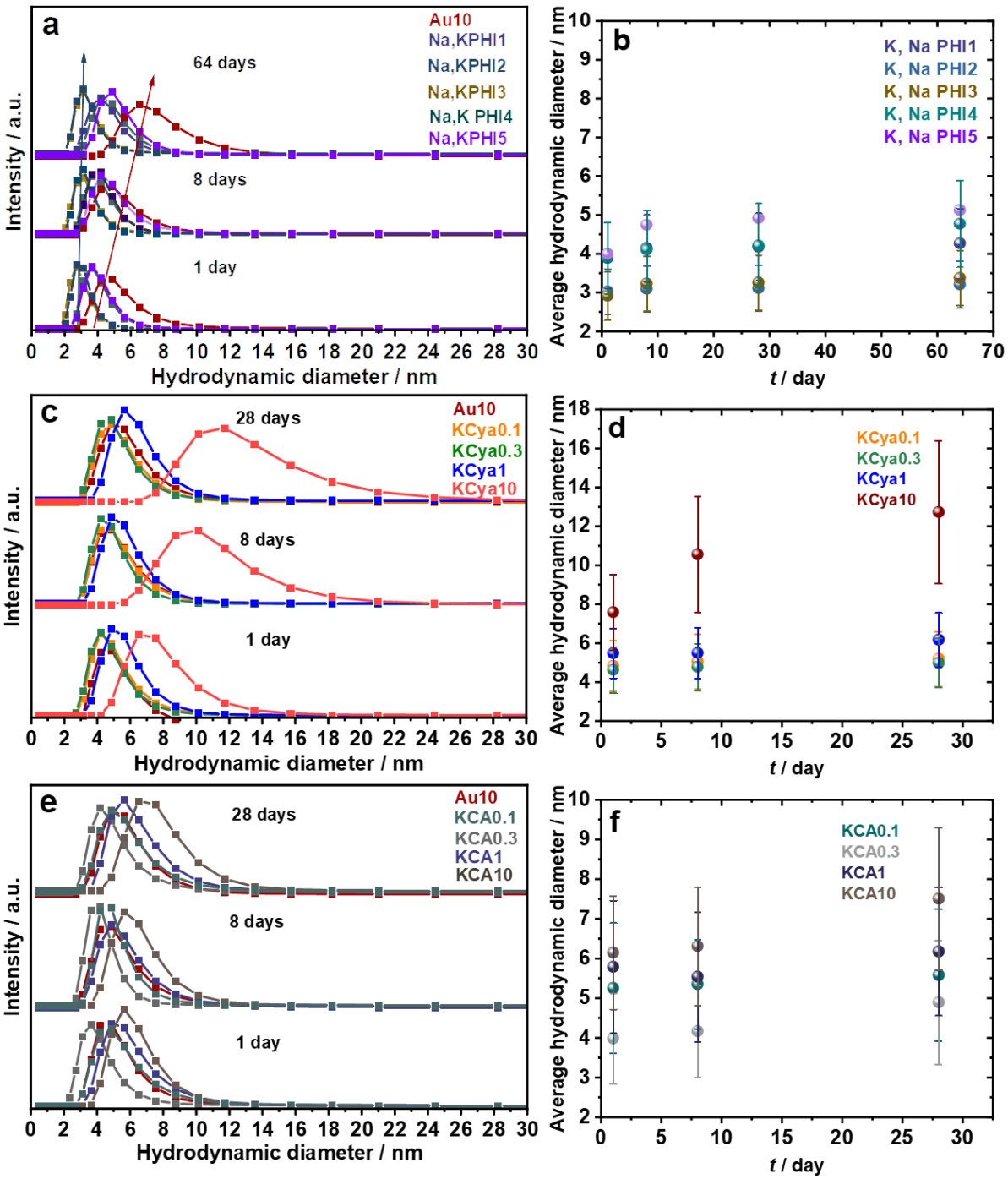

Figure S9. Hydrodynamic diameter determined from the DLS results of Au NPs produced in the presence of different concentrations of (a, b) K, Na PHI, (c, d) KCya, and (e, f) KCA as a function of the storage time.

Stability of Au NPs against heating

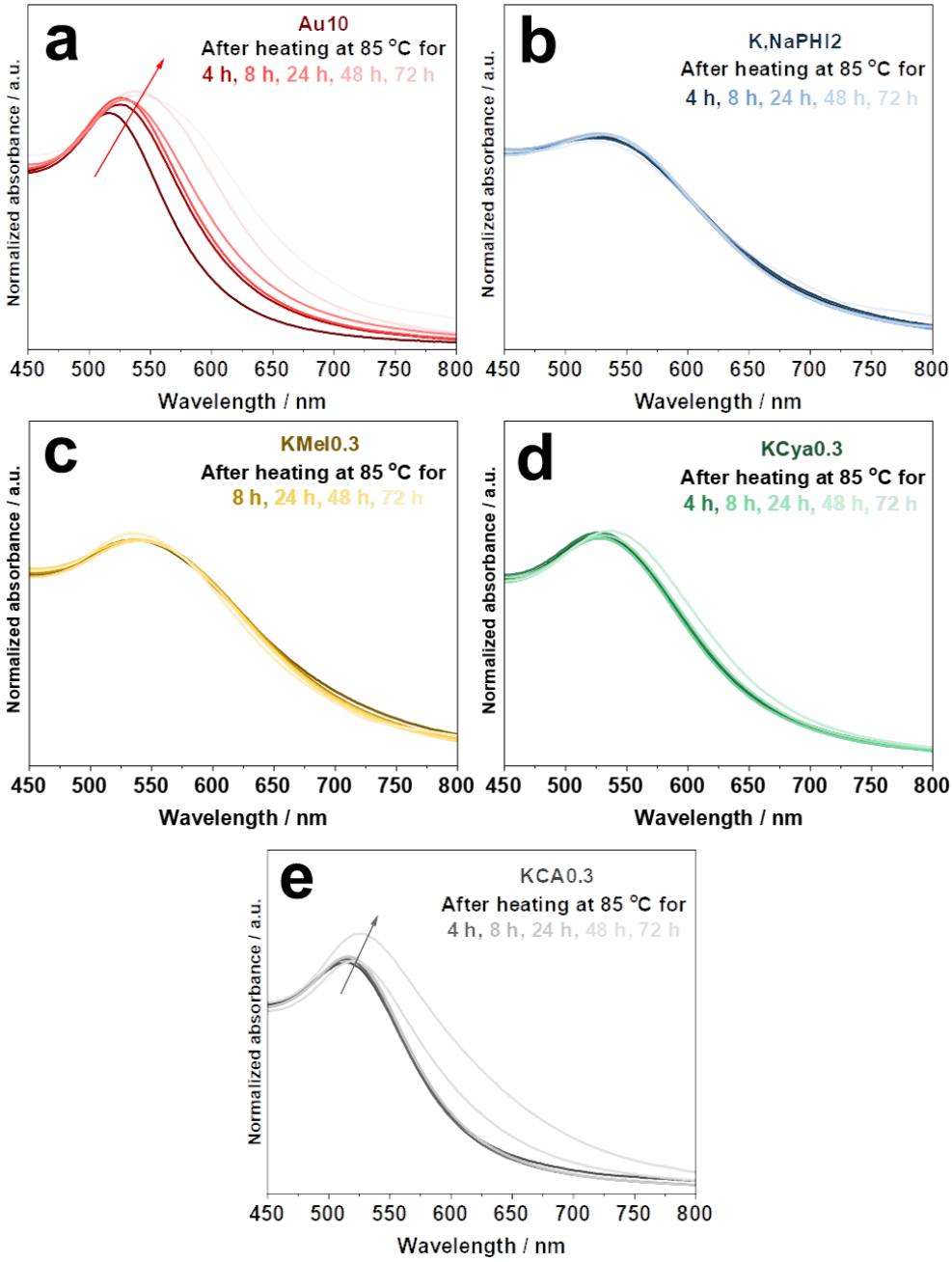

Figure S10. Thermal Stability of Au NPs. (a-e) UV−vis electronic absorption spectra of **Au10**, **K,NaPHI2**, **KMel0.3**, **KCya0.3**, and **KCA0.3** after heating at 85 °C for 4 h, 8 h, 24 h, 48 h, and 72 h.

Note on the effect of reductant-derived impurities on the Au NPs stability

Figure S10 presents the UV-vis spectra, (S)TEM images, and XPS analysis of the **Au10** and the K, Na-PHI-stabilized Au NPs before and after dialysis (_Dial). Upon dialysis, **Au10** is agglomerated as noticed by the broadening of the UV-vis spectrum and the high absorbance intensity at 800 nm (Figure S10a). Similarly, the HAADF-STEM image of **Au10_Dial** reveals that dialysis leads to a complete agglomeration of **Au10 (**Figure S10b,c**)**. This behaviour results from the removal of the excess $NaBH_4$ and consequently, the number of charges around the Au NPs required for electrostatic stabilization is insufficient. In contrast, the UV-vis spectra of the Au NPs stabilized by different concentrations of K, Na-PHI are not significantly changed after dialysis, but the absorbance considerably decreases due to the dilution of the samples during the dialysis process. Furthermore, the average particle size of **K,NaPHI2** is slightly increased after dialysis but it is still below 3 nm, as indicated by the particle size distribution in Figure S11a,b and by comparing the TEM images in Figure S10d,e.

The elemental composition derived from the XPS analysis indicates that the excess $NaBH_4$ from **Au10** and **K,NaPHI2** was removed successfully after dialysis, as demonstrated in Table S3. In the dialyzed samples, no B is detected and the concentration of Na is substantially decreased. The Au $4f_{7/2}$ and Au $4f_{5/2}$ peaks of **Au10** and **K,NaPHI2** are shifted to higher binding energy (by about 0.1 eV) after dialysis (Figure S10f and Table S4). The upshift in the binding energy values after dialysis is due to the change in the chemical environment of the Au NPs into less reductive (removal of the $NaBH_4$ hydrolysis products). On the other hand, dialysis results in no change in the N1s XP spectrum of **K,NaPHI2**.

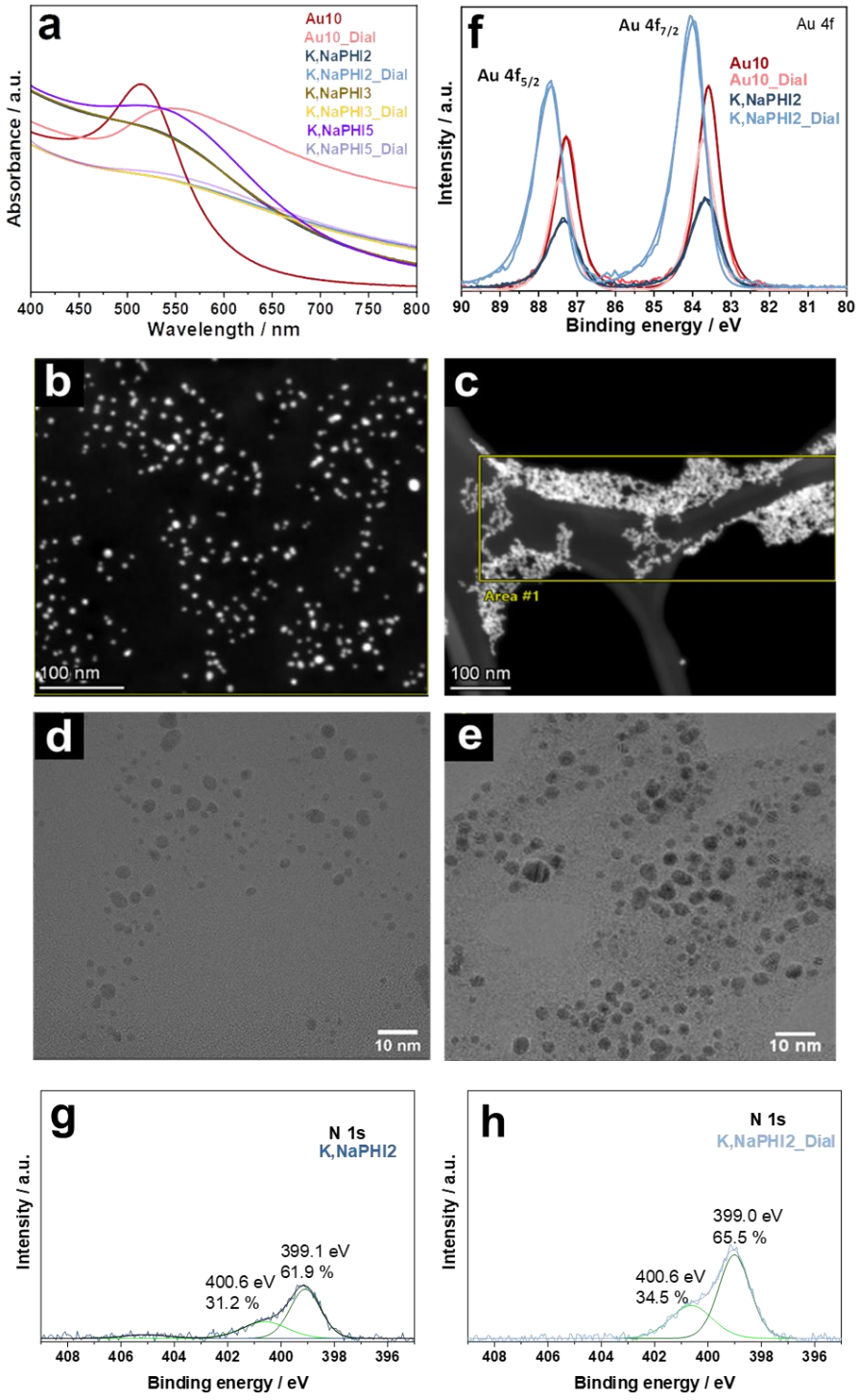

Figure S11. **(a)** UV−vis absorption spectra of **Au10**, **K,NaPHI2**, and **K,NaPHI3** before and after dialysis, HAADF-STEM images of (b) **Au10**, (c) **Au10_Dial**, (d) HRTEM images of **K,NaPHI2**, and **(e) K,NaPHI2_Dial**, (f) XPS spectra of the Au (4f) signal of **Au10** and **K,NaPHI2** before and after dialysis, and (g,h) XPS spectra of the N 1s signal of **K,NaPHI2** before and after dialysis.

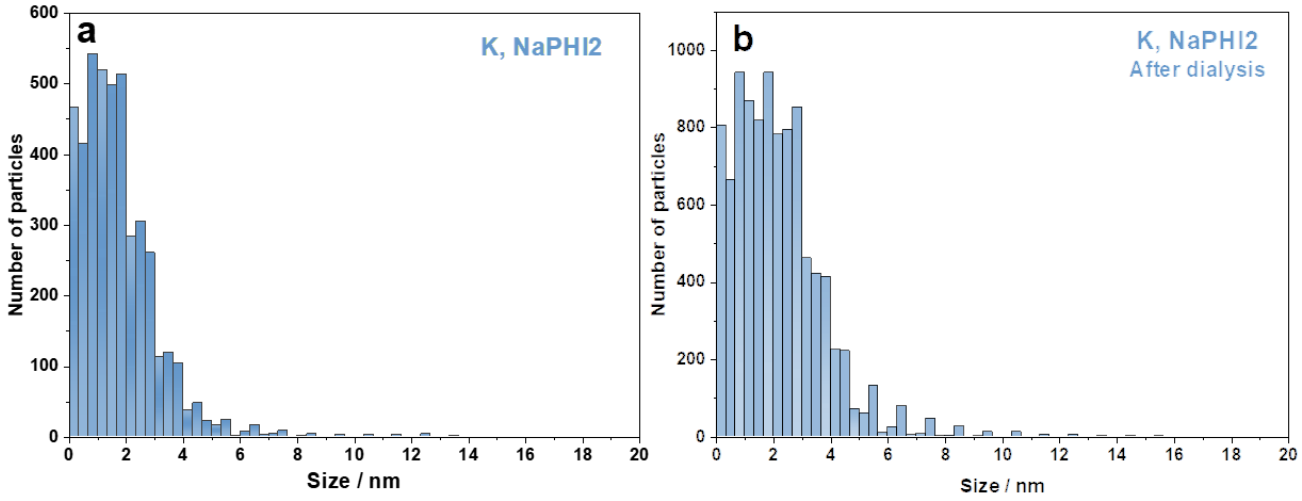

Figure S12. Particle size distribution of **K,NaPHI2** (a) before and (b) after dialysis.

Table S3. Elemental composition derived from the XPS measurements of **Au10** and **K,NaPHI2** before and after dialysis.

Sample	N [%]	Au [%]	Na [%]	B [%]	K [%]	Cl [%]
Au10	-	4	43.1	52.9	-	-
K,NaPHI2	14.2	2	27.9	38.7	3.4	13.7
Au10_Dial	11.8	52.9	35.3	-	-	-
K,NaPHI2_Dial	73.9	19.3	6.8	-	-	-

Table S4. Binding energy and full width at half maximum of the Au 4f for **Au10** and **K,NaPHI2** before and after dialysis.

Sample		Binding energy [eV]	Full width at half maximum [eV]
Au10	Au $4f_{7/2}$	83.6	0.7
	Au $4f_{5/2}$	87.3	
K,NaPHI2	Au $4f_{7/2}$	83.6	0.8
	Au $4f_{5/2}$	87.3	
Au10_Dial	Au $4f_{7/2}$	83.7	0.7
	Au $4f_{5/2}$	87.4	
K,NaPHI2_Dial	Au $4f_{7/2}$	84.0	0.7
	Au $4f_{5/2}$	87.7	

2.3. DFT calculations

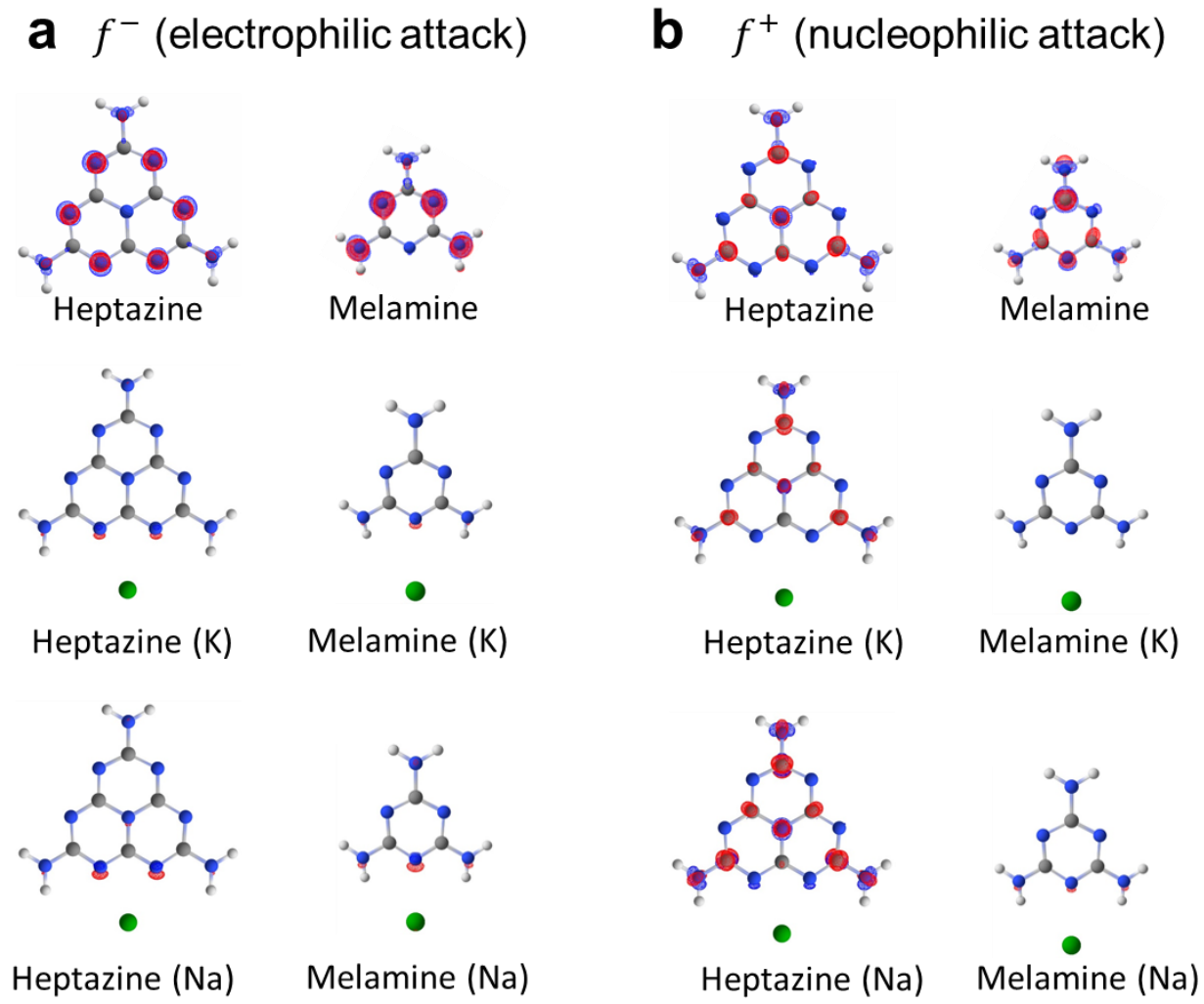

Figure S13. The electron density from Fukui function (a) negative f^- and (b) positive f^+ for (left) heptazine and (right) melamine without the cation (top), with (middle) potassium, and (bottom) sodium.

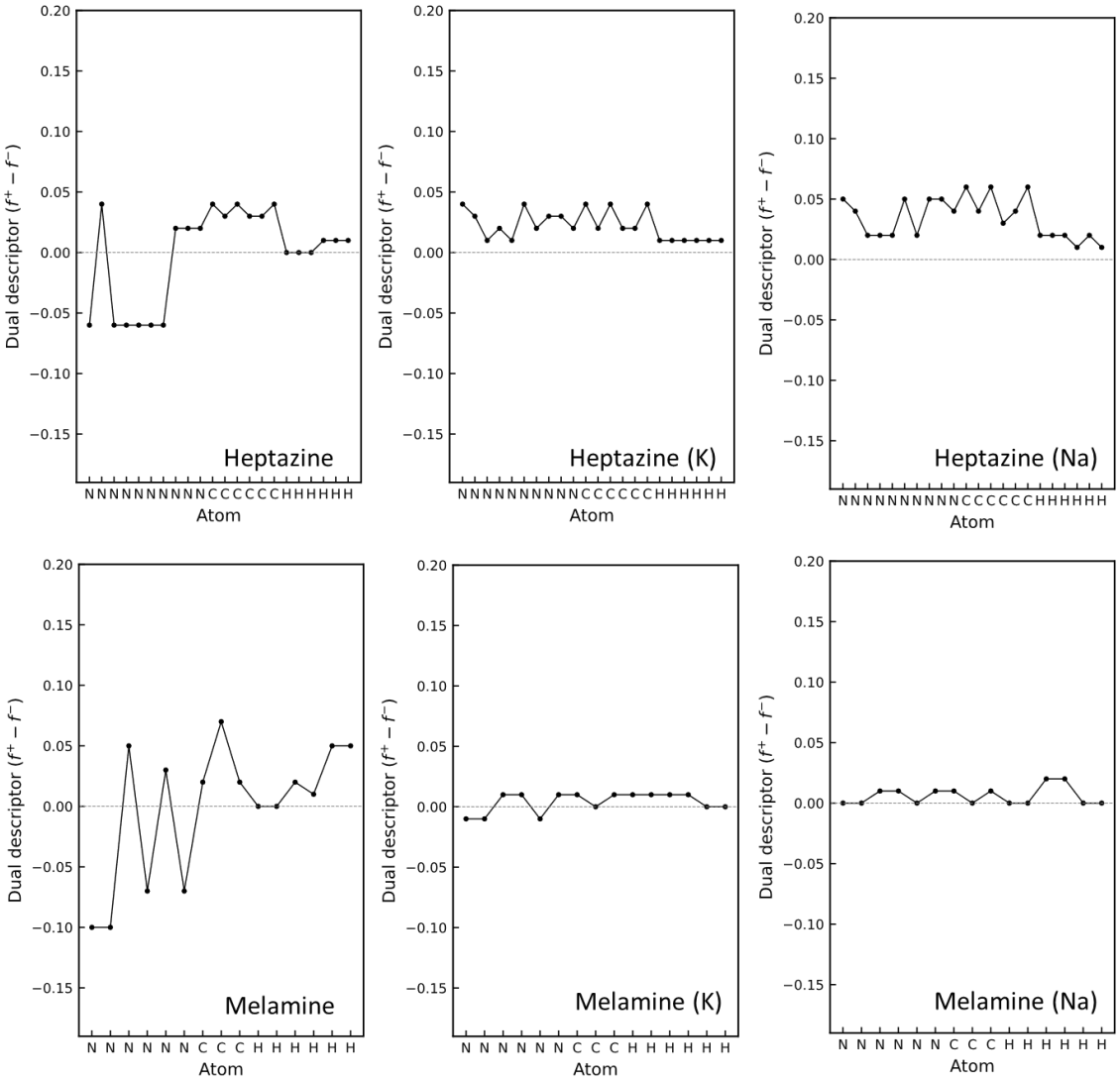

Figure S14. The dual descriptor of heptazine and melamine in the presence of a potassium or a sodium. The negative value corresponds to the electrophilic attack site and the positive value corresponds to the nucleophilic attack site.

Table S5. Fukui function and the dual descriptor from Hirschfeld charge for the carbon nitride species

Cya

Element	Atom Number	*f+*	*f-*	*f0*	*f+-f-*
N	0	-0,10	-0,05	-0,07	-0,05
N	1	-0,01	-0,02	-0,01	0,01
N	2	-0,10	-0,05	-0,07	-0,05
N	3	-0,05	-0,07	-0,06	0,01
N	4	-0,05	-0,07	-0,06	0,02
N	5	-0,08	-0,06	-0,07	-0,01
N	6	-0,07	-0,06	-0,07	-0,01
O	7	-0,19	-0,10	-0,15	-0,08
O	8	-0,09	-0,17	-0,13	0,08
O	9	-0,09	-0,15	-0,12	0,06
C	10	-0,03	-0,05	-0,04	0,02
C	11	-0,02	-0,02	-0,02	0,01
C	12	-0,03	-0,05	-0,04	0,02
C	13	-0,02	-0,03	-0,02	0,00
C	14	-0,02	-0,02	-0,02	0,00
C	15	-0,05	-0,03	-0,04	-0,02

K1Cya

Element	Atom Number	*f+*	*f-*	*f0*	*f+-f-*
N	0	-0,13	-0,03	-0,08	-0,10
N	1	-0,01	-0,01	-0,01	0,00
N	2	-0,11	-0,03	-0,07	-0,08
N	3	-0,04	-0,11	-0,07	0,06
N	4	-0,05	-0,14	-0,10	0,09
N	5	-0,12	-0,06	-0,09	-0,07
N	6	-0,07	-0,06	-0,06	0,00
O	7	-0,11	-0,08	-0,09	-0,02
O	8	-0,07	-0,13	-0,10	0,07
O	9	-0,08	-0,12	-0,10	0,04
C	10	-0,03	-0,04	-0,03	0,01
C	11	-0,02	-0,03	-0,02	0,02
C	12	-0,03	-0,04	-0,03	0,01
C	13	-0,03	-0,02	-0,02	-0,01
C	14	-0,02	-0,02	-0,02	-0,01
C	15	-0,04	-0,02	-0,03	-0,02
K	16	-0,06	-0,05	-0,06	0,00

K2Cya

Element	Atom Number	*f+*	*f-*	*f0*	*f+-f-*
N	0	-0,11	-0,08	-0,09	-0,02
N	1	0,00	0,00	0,00	0,00
N	2	-0,06	-0,10	-0,08	0,04
N	3	-0,07	-0,06	-0,06	-0,01
N	4	-0,06	-0,08	-0,07	0,02
N	5	-0,17	-0,07	-0,12	-0,10
N	6	-0,09	-0,11	-0,10	0,03
O	7	-0,08	-0,12	-0,10	0,05
O	8	-0,05	-0,06	-0,05	0,02
O	9	-0,05	-0,06	-0,06	0,01
C	10	-0,03	-0,03	-0,03	0,00
C	11	-0,02	-0,02	-0,02	0,00
C	12	-0,03	-0,02	-0,02	0,00
C	13	-0,03	-0,02	-0,03	-0,02
C	14	-0,02	-0,02	-0,02	0,00
C	15	-0,03	-0,04	-0,04	0,01
K	16	-0,05	-0,04	-0,05	-0,01
K	17	-0,06	-0,05	-0,06	-0,01

K3Cya0.3

Element	Atom Number	*f+*	*f-*	*f0*	*f+-f-*
N	0	-0,01	-0,13	-0,07	0,12
N	1	0,00	0,00	0,00	0,00
N	2	0,01	-0,05	-0,02	0,07
N	3	-0,01	-0,07	-0,04	0,06
N	4	-0,01	-0,08	-0,04	0,07
N	5	-0,01	-0,12	-0,07	0,11
N	6	0,01	-0,06	-0,02	0,07
O	7	0,00	-0,06	-0,03	0,06
O	8	-0,02	-0,06	-0,04	0,04
O	9	0,00	-0,05	-0,03	0,05
C	10	-0,01	-0,03	-0,02	0,02
C	11	0,00	-0,02	-0,01	0,01
C	12	0,00	-0,02	-0,01	0,02
C	13	0,00	-0,03	-0,02	0,02
C	14	0,00	-0,01	-0,01	0,01
C	15	0,00	-0,03	-0,02	0,03
K	16	-0,02	-0,06	-0,04	0,04
K	17	-0,50	-0,05	-0,27	-0,45
K	18	-0,42	-0,06	-0,24	-0,37

CA

Element	Atom Number	*f+*	*f-*	*f0*	*f+-f-*
N	0	-0,18	-0,09	-0,14	-0,09
N	1	-0,11	-0,09	-0,10	-0,01
N	2	-0,11	-0,09	-0,10	-0,02
O	3	-0,16	-0,17	-0,16	0,01
O	4	-0,16	-0,17	-0,16	0,00
O	5	-0,12	-0,21	-0,17	0,09
C	6	-0,06	-0,05	-0,06	-0,01
C	7	-0,06	-0,05	-0,06	-0,01
C	8	-0,04	-0,07	-0,05	0,03

K1CA

Element	Atom Number	*f+*	*f-*	*f0*	*f+-f-*
N	0	0,02	-0,07	-0,03	0,08
N	1	-0,01	-0,15	-0,08	0,14
N	2	-0,02	-0,14	-0,08	0,13
O	3	-0,02	-0,20	-0,11	0,18
O	4	0,01	-0,12	-0,05	0,12
O	5	-0,02	-0,12	-0,07	0,10
C	6	-0,01	-0,05	-0,03	0,05
C	7	0,00	-0,04	-0,02	0,04
C	8	-0,01	-0,05	-0,03	0,04
K	9	-0,93	-0,06	-0,49	-0,86

K2CA

Element	Atom Number	*f+*	*f-*	*f0*	*f+-f-*
N	0	-0,02	-0,17	-0,10	0,15
N	1	-0,11	-0,06	-0,08	-0,04
N	2	-0,04	-0,12	-0,08	0,08
O	3	-0,04	-0,08	-0,06	0,04
O	4	-0,05	-0,18	-0,12	0,13
O	5	-0,01	-0,10	-0,05	0,09
C	6	-0,02	-0,03	-0,03	0,02
C	7	-0,02	-0,05	-0,04	0,03
C	8	-0,02	-0,04	-0,03	0,03
K	9	-0,06	-0,08	-0,07	0,02
K	10	-0,61	-0,06	-0,34	-0,55

K3CA

Element	Atom Number	*f+*	*f-*	*f0*	*f+-f-*
N	0	0,00	-0,06	-0,03	0,06
N	1	0,00	-0,19	-0,09	0,19
N	2	0,00	-0,07	-0,03	0,07
O	3	0,00	-0,16	-0,08	0,15
O	4	0,00	-0,09	-0,04	0,08
O	5	0,00	-0,08	-0,04	0,08
C	6	0,00	-0,04	-0,02	0,03
C	7	0,00	-0,03	-0,02	0,03
C	8	0,00	-0,04	-0,02	0,03
K	9	-0,32	-0,08	-0,20	-0,24
K	10	-0,32	-0,08	-0,20	-0,24
K	11	-0,32	-0,09	-0,21	-0,24

Mel

Element	Atom Number	*f+*	*f-*	*f0*	*f+-f-*
N	0	-0,03	-0,10	-0,06	0,07
N	1	-0,03	0,00	-0,01	-0,03
N	2	-0,01	-0,07	-0,04	0,06
N	3	-0,02	-0,09	-0,06	0,07
N	4	-0,03	-0,08	-0,06	0,05
N	5	-0,05	-0,09	-0,07	0,04
N	6	0,00	-0,07	-0,04	0,07
N	7	-0,09	-0,01	-0,05	-0,08
N	8	-0,01	-0,01	-0,01	0,00
N	9	-0,09	-0,01	-0,05	-0,08
N	10	-0,06	-0,07	-0,06	0,01
N	11	-0,15	-0,08	-0,11	-0,07
N	12	-0,14	-0,08	-0,11	-0,06
C	13	-0,02	-0,02	-0,02	0,00
C	14	-0,02	-0,02	-0,02	0,00
C	15	-0,03	-0,03	-0,03	0,00
C	16	-0,02	-0,02	-0,02	0,00
C	17	-0,02	-0,02	-0,02	0,00
C	18	-0,03	-0,03	-0,03	0,00
C	19	-0,06	-0,03	-0,05	-0,03
C	20	-0,06	-0,03	-0,05	-0,03
C	21	-0,02	-0,02	-0,02	0,00

K1Mel

Element	Atom Number	*f+*	*f-*	*f0*	*f+-f-*
N	0	-0,03	-0,06	-0,05	0,03
N	1	-0,02	-0,02	-0,02	0,00
N	2	-0,01	-0,03	-0,02	0,02
N	3	-0,02	-0,02	-0,02	0,00
N	4	-0,03	-0,02	-0,03	-0,01
N	5	-0,06	-0,03	-0,05	-0,03
N	6	0,00	-0,06	-0,03	0,06
N	7	-0,07	-0,01	-0,04	-0,06
N	8	-0,03	-0,13	-0,08	0,10
N	9	-0,12	-0,01	-0,07	-0,11
N	10	-0,06	-0,19	-0,12	0,13
N	11	-0,16	-0,05	-0,11	-0,11
N	12	-0,12	-0,06	-0,09	-0,06
C	13	-0,01	-0,02	-0,02	0,01
C	14	-0,01	-0,02	-0,01	0,00
C	15	-0,02	-0,02	-0,02	0,00
C	16	-0,02	-0,02	-0,02	0,00
C	17	-0,02	-0,02	-0,02	0,00
C	18	-0,02	-0,02	-0,02	0,00
C	19	-0,06	-0,02	-0,04	-0,04
C	20	-0,05	-0,02	-0,04	-0,02
C	21	-0,01	-0,08	-0,05	0,07
K	22	-0,03	-0,04	-0,04	0,02

K2Mel

Element	Atom Number	*f+*	*f-*	*f0*	*f+-f-*
N	0	-0,04	-0,01	-0,02	-0,03
N	1	-0,01	-0,01	-0,01	0,00
N	2	-0,02	-0,02	-0,02	0,00
N	3	-0,02	-0,05	-0,04	0,03
N	4	-0,02	-0,05	-0,04	0,03
N	5	-0,05	-0,02	-0,04	-0,04
N	6	-0,01	-0,03	-0,02	0,03
N	7	-0,18	-0,02	-0,10	-0,16
N	8	-0,03	-0,10	-0,06	0,06
N	9	-0,02	-0,08	-0,05	0,06
N	10	-0,05	-0,15	-0,10	0,10
N	11	-0,05	-0,11	-0,08	0,06
N	12	-0,23	-0,06	-0,14	-0,18
C	13	-0,01	-0,02	-0,02	0,01
C	14	-0,01	-0,02	-0,01	0,01
C	15	-0,01	-0,02	-0,01	0,01
C	16	-0,02	-0,01	-0,02	-0,01
C	17	-0,02	-0,01	-0,01	0,00
C	18	-0,03	-0,02	-0,02	-0,01
C	19	-0,01	-0,04	-0,02	0,03
C	20	-0,09	-0,02	-0,06	-0,07
C	21	-0,01	-0,06	-0,04	0,05
K	22	-0,03	-0,04	-0,04	0,01
K	23	-0,02	-0,04	-0,03	0,01

K3Mel

Element	Atom Number	*f+*	*f-*	*f0*	*f+-f-*
N	0	0,00	-0,03	-0,01	0,03
N	1	0,00	-0,01	0,00	0,00
N	2	0,00	-0,02	-0,01	0,02
N	3	0,00	-0,03	-0,01	0,03
N	4	0,00	-0,05	-0,02	0,04
N	5	0,00	-0,05	-0,02	0,05
N	6	0,00	-0,02	-0,01	0,01
N	7	0,00	-0,05	-0,03	0,05
N	8	0,00	-0,09	-0,05	0,09
N	9	0,00	-0,06	-0,03	0,06
N	10	-0,02	-0,13	-0,07	0,11
N	11	-0,02	-0,09	-0,05	0,07
N	12	-0,02	-0,09	-0,05	0,08
C	13	0,00	-0,02	-0,01	0,02
C	14	0,00	-0,01	-0,01	0,01
C	15	0,00	-0,01	-0,01	0,01
C	16	0,00	-0,01	-0,01	0,01
C	17	0,00	-0,01	-0,01	0,01
C	18	0,00	-0,01	-0,01	0,01
C	19	0,00	-0,03	-0,02	0,03
C	20	0,00	-0,03	-0,02	0,03
C	21	0,00	-0,05	-0,03	0,05
K	22	-0,31	-0,04	-0,18	-0,27
K	23	-0,31	-0,03	-0,17	-0,28
K	24	-0,32	-0,03	-0,17	-0,28

hep

Element	Atom Number	*f+*	*f-*	*f0*	*f+-f-*
N	0	-0,04	-0,10	-0,07	0,06
N	1	-0,04	0,00	-0,02	-0,04
N	2	-0,04	-0,10	-0,07	0,06
N	3	-0,04	-0,10	-0,07	0,06
N	4	-0,04	-0,10	-0,07	0,06
N	5	-0,04	-0,10	-0,07	0,06
N	6	-0,04	-0,10	-0,07	0,06
N	7	-0,06	-0,04	-0,05	-0,02
N	8	-0,06	-0,04	-0,05	-0,02
N	9	-0,06	-0,04	-0,05	-0,02
C	10	-0,07	-0,03	-0,05	-0,04
C	11	-0,05	-0,02	-0,03	-0,03
C	12	-0,07	-0,03	-0,05	-0,04
C	13	-0,05	-0,02	-0,03	-0,02
C	14	-0,05	-0,02	-0,03	-0,03
C	15	-0,07	-0,03	-0,05	-0,04
H	16	-0,03	-0,03	-0,03	-0,01
H	17	-0,03	-0,03	-0,03	-0,01
H	18	-0,03	-0,03	-0,03	-0,01
H	19	-0,03	-0,02	-0,03	-0,01
H	20	-0,03	-0,02	-0,03	-0,01
H	21	-0,03	-0,02	-0,03	-0,01

hepK

Element	Atom Number	*f+*	*f-*	*f0*	*f+-f-*
N	0	-0,02	0,02	0,00	-0,03
N	1	-0,03	0,00	-0,01	-0,02
N	2	-0,03	-0,02	-0,02	-0,01
N	3	-0,03	-0,01	-0,02	-0,01
N	4	-0,03	-0,02	-0,02	-0,01
N	5	-0,02	0,02	0,00	-0,03
N	6	-0,03	-0,01	-0,02	-0,01
N	7	-0,04	-0,01	-0,02	-0,03
N	8	-0,04	-0,01	-0,02	-0,03
N	9	-0,04	-0,02	-0,03	-0,02
C	10	-0,04	0,00	-0,02	-0,04
C	11	-0,03	-0,01	-0,02	-0,03
C	12	-0,05	-0,01	-0,03	-0,04
C	13	-0,02	0,00	-0,01	-0,02
C	14	-0,03	-0,01	-0,02	-0,03
C	15	-0,04	0,00	-0,02	-0,04
H	16	-0,02	-0,01	-0,02	-0,01
H	17	-0,02	-0,01	-0,02	-0,01
H	18	-0,02	-0,01	-0,02	-0,01
H	19	-0,02	-0,01	-0,02	-0,01
H	20	-0,02	-0,01	-0,02	-0,01
H	21	-0,02	-0,01	-0,02	-0,01
K	22	-0,36	-0,84	-0,60	0,47

hepNa

Element	Atom Number	*f+*	*f-*	*f0*	*f+-f-*
N	0	-0,03	0,02	-0,01	-0,05
N	1	-0,04	0,00	-0,02	-0,04
N	2	-0,04	-0,02	-0,03	-0,02
N	3	-0,04	-0,02	-0,03	-0,02
N	4	-0,04	-0,02	-0,03	-0,02
N	5	-0,03	0,02	-0,01	-0,05
N	6	-0,04	-0,02	-0,03	-0,02
N	7	-0,05	0,00	-0,03	-0,05
N	8	-0,05	0,00	-0,03	-0,05
N	9	-0,06	-0,02	-0,04	-0,04
C	10	-0,06	0,00	-0,03	-0,06
C	11	-0,05	-0,01	-0,03	-0,04
C	12	-0,07	-0,01	-0,04	-0,06
C	13	-0,03	0,00	-0,02	-0,03
C	14	-0,05	-0,01	-0,03	-0,04
C	15	-0,06	0,00	-0,03	-0,06
H	16	-0,03	-0,01	-0,02	-0,02
H	17	-0,03	-0,01	-0,02	-0,02
H	18	-0,03	-0,01	-0,02	-0,02
H	19	-0,02	-0,01	-0,02	-0,01
H	20	-0,03	-0,01	-0,02	-0,02
H	21	-0,02	-0,01	-0,02	-0,02
Na	22	-0,10	-0,86	-0,48	0,75

mel

Element	Atom Number	*f+*	*f-*	*f0*	*f+-f-*
N	0	-0,05	-0,15	-0,10	0,09
N	1	-0,05	-0,15	-0,10	0,10
N	2	-0,09	-0,04	-0,06	-0,05
N	3	-0,05	-0,12	-0,09	0,07
N	4	-0,08	-0,05	-0,06	-0,03
N	5	-0,05	-0,12	-0,09	0,07
C	6	-0,06	-0,04	-0,05	-0,02
C	7	-0,11	-0,04	-0,08	-0,08
C	8	-0,06	-0,04	-0,05	-0,02
H	9	-0,05	-0,05	-0,05	0,00
H	10	-0,05	-0,05	-0,05	0,00
H	11	-0,07	-0,05	-0,06	-0,02
H	12	-0,06	-0,05	-0,06	-0,01
H	13	-0,08	-0,03	-0,06	-0,05
H	14	-0,08	-0,03	-0,06	-0,05

melK

Element	Atom Number	*f+*	*f-*	*f0*	*f+-f-*
N	0	-0,01	-0,02	-0,01	0,00
N	1	-0,01	-0,02	-0,01	0,00
N	2	0,01	0,02	0,01	-0,01
N	3	-0,01	0,00	0,00	-0,01
N	4	-0,01	-0,02	-0,02	0,00
N	5	-0,01	0,00	0,00	-0,01
C	6	-0,01	0,00	0,00	0,00
C	7	-0,01	-0,01	-0,01	0,00
C	8	-0,01	0,00	0,00	0,00
H	9	-0,02	-0,01	-0,02	-0,01
H	10	-0,02	-0,01	-0,02	-0,01
H	11	-0,02	-0,01	-0,02	-0,01
H	12	-0,02	-0,01	-0,02	-0,01
H	13	-0,01	-0,01	-0,01	0,00
H	14	-0,01	-0,01	-0,01	0,00
K	15	-0,82	-0,89	-0,85	0,07

melNa

Element	Atom Number	*f+*	*f-*	*f0*	*f+-f-*
N	0	-0,02	-0,02	-0,02	0,00
N	1	-0,02	-0,02	-0,02	0,00
N	2	0,01	0,02	0,01	-0,01
N	3	-0,01	0,00	-0,01	-0,01
N	4	-0,02	-0,02	-0,02	0,00
N	5	-0,01	0,00	-0,01	-0,01
C	6	-0,01	0,00	-0,01	-0,01
C	7	-0,01	-0,01	-0,01	0,00
C	8	-0,01	0,00	-0,01	-0,01
H	9	-0,02	-0,02	-0,02	-0,01
H	10	-0,02	-0,02	-0,02	-0,01
H	11	-0,03	-0,01	-0,02	-0,02
H	12	-0,03	-0,01	-0,02	-0,02
H	13	-0,01	-0,01	-0,01	0,00
H	14	-0,01	-0,01	-0,01	0,00
Na	15	-0,77	-0,85	-0,81	0,09

2.4. Catalytic reduction of 4-NP

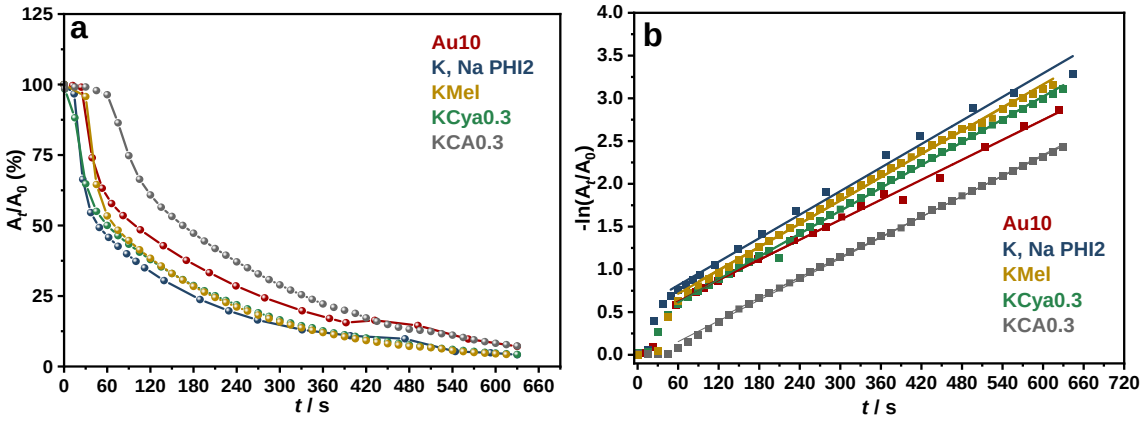

Figure S15. (a) Comparative catalytic conversion of 4-NP with **Au10**, **K,NaPHI2**, **KMel0.3**, **KCA0.3**, and **KCya0.3**. (b) Plots of ln (A_t/A_0) for the absorbance of nitrophenolate anion at 400 nm obtained from the spectra versus time for the reduction of 4-NP catalyzed by the catalysts **Au10**, **K,NaPHI2**, **KMel0.3**, **KCA0.3**, and **KCya0.3**. *Experimental conditions*: 0.1 mL $NaBH_4$ (2.16 mol L^{-1}), 0.3 mL 4-NP (1.2×10^{-3} mol L^{-1}), and 2.5 mL distilled water were mixed into a cuvette at ambient conditions. Then, the UV-Vis spectrum was recorded, followed by the addition of 0.025 mL of AuNP catalyst (1.14 mg L^{-1}) and shaking quickly the cuvette before recording the subsequent spectra.

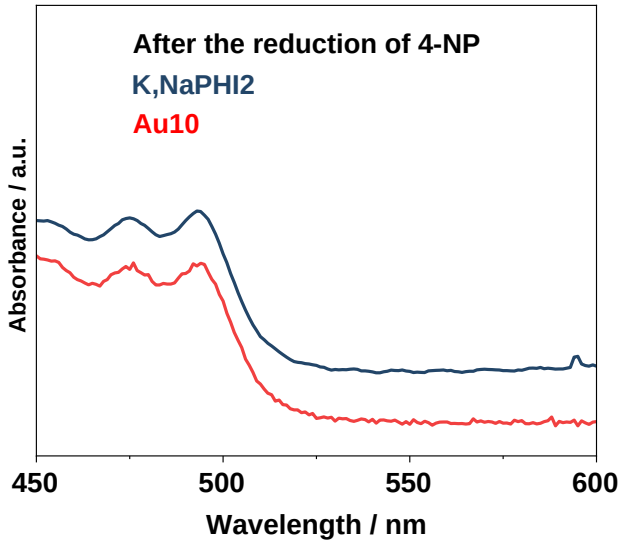

Figure S16. UV−vis electronic absorption spectra of **Au10** and **K,NaPHI2** after the reduction of 4-NP under the reaction conditions specified in the caption of Figure S15.

References

1 I. Krivtsov, D. Mitoraj, C. Adler, M. Ilkaeva, M. Sardo, L. Mafra, C. Neumann, A. Turchanin, C. Li, B. Dietzek, R. Leiter, J. Biskupek, U. Kaiser, C. Im, B. Kirchhoff, T. Jacob and R. Beranek, *Angew. Chem. Int. Ed.*, 2020, **59**, 487-495.

2 H. Schlomberg, J. Kröger, G. Savasci, M. W. Terban, S. Bette, I. Moudrakovski, V. Duppel, F. Podjaski, R. Siegel, J. Senker, R. E. Dinnebier, C. Ochsenfeld and B. v. Lotsch, *Chem. Mater.*, 2019, **31**, 7478–7486.

3 C. Deraedt, L. Salmon, S. Gatard, R. Ciganda, R. Hernandez, M. Mayor and D. Astruc, *ChemComm.*, 2014, **50**, 14194–14196.

4 L. Guardia, J. I. Paredes, J. M. Munuera, S. Villar-Rodil, M. Ayán-Varela, A. Martínez-Alonso and J. M. D. Tascón, *ACS Appl. Mater. Interfaces*, 2014, **6**, 21702–21710.

5 S. García-Dalí, J. I. Paredes, S. Villar-Rodil, A. Martínez-Jódar, A. Martínez-Alonso and J. M. D. Tascón, *ACS Appl. Mater. Interfaces*, 2021, **13**, 33157–33171.

6 F. Neese, *WIREs Computational Molecular Science*, 2012, **2**, 73–78.

7 F. Neese, F. Wennmohs, U. Becker and C. Riplinger, *J. Chem. Phys.*, 2020, **152**, 224108-.

8 J. Heyd, G. E. Scuseria and M. Ernzerhof, *J. Chem. Phys.*, 2003, **118**, 8207–8215.

9 J. P. Perdew, M. Ernzerhof and K. Burke, *J. Chem. Phys.*, 1996, **105**, 9982–9985.

10 C. Adamo and V. Barone, *J Chem Phys*, 1999, **110**, 6158–6170.

11 A. D. McNaught and A. Wilkinson, *Compendium of chemical terminology*, Blackwell Science Oxford, 1997, vol. 1669.

12 R. R. Contreras, P. Fuentealba, M. Galván and P. Pérez, *Chem. Phys. Lett.*, 1999, **304**, 405–413.

13 W. Yang and R. G. Parr, *Proc. Natl. Acad. Sci.*, 1985, **82**, 6723–6726.

14 B. M. Quinn, P. Liljeroth, V. Ruiz, T. Laaksonen and K. Kontturi, *J. Am. Chem. Soc.*, 2003, **125**, 6644–6645.

15 K. B. Male, J. Li, C. C. Bun, S.-C. Ng and J. H. T. Luong, *J. Phys. Chem. C*, 2008, **112**, 443–451.

16 I. Hussain, S. Graham, Z. Wang, B. Tan, D. C. Sherrington, S. P. Rannard, A. I. Cooper and M. Brust, *J. Am. Chem. Soc.*, 2005, **127**, 16398–16399.

17 J. A. Creighton and D. G. Eadon, *J. Chem. Soc., Faraday Trans.*, 1991, **87**, 3881–3891.

18 X. Wang, W. Zhang, X. Gong, X. Hu and X. Yao, *J. Nanopart. Res.*, 2019, **21**, 192.

19 M. Šetka, R. Calavia, L. Vojkůvka, E. Llobet, J. Drbohlavová and S. Vallejos, *Sci. Rep.*, 2019, **9**, 8465.